

Article

Increasing Electrical Resistivity of P-Type BiFeO₃ Ceramics by Hydrogen Peroxide-Assisted Hydrothermal Synthesis

Cristian Casut ^{1,2} , Raul Bucur ¹, Daniel Ursu ¹ , Iosif Malaescu ^{2,3}  and Marinela Miclau ^{1,*}

¹ National Institute for Research and Development in Electrochemistry and Condensed Matter, Plautius Andronescu Str, No. 1, 300224 Timisoara, Romania

² Physics Faculty, West University of Timisoara, V. Pârvan Ave., No. 4, 300223 Timisoara, Romania

³ Institute for Advanced Environmental Research, West University of Timisoara (ICAM-WUT), Oituz Str., No. 4, 300086 Timisoara, Romania

* Correspondence: marinela.miclau@gmail.com

Abstract: Bismuth ferrite (BiFeO₃, BFO) is still widely investigated both because of the great diversity of its possible applications and from the perspective of intrinsic defect engineering in the perovskite structure. Defect control in BiFeO₃ semiconductors could provide a key technology for overcoming undesirable limitations, namely, a strong leakage current, which is attributed to the presence of oxygen vacancies (V_O) and Bi vacancies (V_{Bi}). Our study proposes a hydrothermal method for the reduction of the concentration of V_{Bi} during the ceramic synthesis of BiFeO₃. Using hydrogen peroxide (H₂O₂) as part of the medium, *p*-type BiFeO₃ ceramics characterized by their low conductivity were obtained. Hydrogen peroxide acted as the electron donor in the perovskite structure, controlling V_{Bi} in the BiFeO₃ semiconductor, which caused the dielectric constant and loss to decrease along with the electrical resistivity. The reduction of Bi vacancies highlighted by a FT-IR and Mott—Schottky analysis has an expected contribution to the dielectric characteristic. A decrease in the dielectric constant (with approximately 40%) and loss (3 times) and an increase of the electrical resistivity (by 3 times) was achieved by the hydrogen peroxide-assisted hydrothermal synthesized BFO ceramics, as compared with the hydrothermal synthesized BFOs.



Citation: Casut, C.; Bucur, R.; Ursu, D.; Malaescu, I.; Miclau, M.

Increasing Electrical Resistivity of P-Type BiFeO₃ Ceramics by Hydrogen Peroxide-Assisted Hydrothermal Synthesis. *Materials*

2023, 16, 3130. <https://doi.org/10.3390/ma16083130>

Academic Editor: Andres Sotelo

Received: 6 March 2023

Revised: 10 April 2023

Accepted: 13 April 2023

Published: 16 April 2023



Copyright: © 2023 by the authors. Licensee MDPI, Basel, Switzerland. This article is an open access article distributed under the terms and conditions of the Creative Commons Attribution (CC BY) license (<https://creativecommons.org/licenses/by/4.0/>).

1. Introduction

Bismuth ferrite (BiFeO₃, BFO) is being widely investigated because of the great diversity of its possible applications that offer a wide range of potentially new applications including spintronics [1], new data storage media [2], multiple-state memories [3,4], ferroelectric diode devices [5], ferroelectric photovoltaics [6,7] or as a photoelectrode in a solar water-splitting cell [8].

However, its commercialization is conditioned by the tendency to exhibit strong leakage currents, which have often been attributed to the presence of oxygen vacancies (V_O) [9,10] and Bi vacancies (V_{Bi}) [11]. If oxygen vacancies dominate the conductivity of BFO under oxygen-poor conditions, determining *n*-type behavior [12–15], Bi vacancies play a dominant role under oxygen-rich conditions, causing *p*-type conductivity of BFO [16].

Besides its potential applications, the defect control in BiFeO₃ semiconductors is also interesting and fascinating and could provide a key technology for overcoming undesirable limitations. So far, many papers have mainly focused on studying the oxygen vacancies and their reduction in correlation with the properties as the main defects in BFO thin films and ceramics [17,18]. It has been reported that oxygen vacancies can be reduced through doping or treatment in an oxygen atmosphere; thus, an increase in the effective resistance has been highlighted [19,20]. From this perspective, using hydrogen peroxide as oxygen

sources in the solutions was explored for the reduction of the concentration of oxygen vacancies presented in *n*-type BFO [21].

However, few studies on V_{Bi} in BFO thin films and ceramics have been published, especially from the perspective of first-principles density functional calculations [22,23]. In accordance with theoretical calculations, the most stable state for V_{Bi} is the fully ionized one, V_{Bi}^{3-} , obtained by release of their holes, which determined the *p*-type conduction. Thus, BiFeO_3 acts as a *p*-type semiconductor with a high concentration of h^+ . As a result, the conductivity of BFO can be reduced by decreasing the concentration of V_{Bi} through two mechanisms, namely, increasing the donor concentration or decreasing the acceptor concentration. To our knowledge, one study reported that the conductivity of *p*-type BFO decreased through the reduction of the concentration of V_{Bi} due to the doping of BFO nanofibers with Sn by the sol–gel electrospinning technique [16].

In this paper, we propose a reduction of the concentration of V_{Bi} during the synthesis of BFO ceramics. Thus, using hydrogen peroxide (H_2O_2) as part of a hydrothermal medium, *p*-type BiFeO_3 ceramics characterized by low conductivity have been obtained. In accordance with our study, hydrogen peroxide acted as an electron donor in the perovskite structure, controlling the defects in the BiFeO_3 semiconductor.

2. Materials and Methods

In a typical hydrothermal synthesis described in our earlier work [24], we were able to produce BiFeO_3 (BFO). Sample 1 (S1), which will be used as a reference, was obtained by separately mixing, 1 mmol (0.5 g) of bismuth nitrate ($\text{Bi}(\text{NO}_3)_3 \times 5\text{H}_2\text{O} \geq 98\%$) and 1 mmol (0.4 g) of ferric nitrate ($\text{Fe}(\text{NO}_3)_3 \times 9\text{H}_2\text{O} \geq 98\%$) in 5 mL distilled water. Both solutions were then homogenized for 15 min using magnetic stirring, generating a brownish-yellow solution. The sample mixture was combined with a 10 mL of 1 M sodium hydroxide ($\text{Na(OH)} \geq 99\%$) solution before being transferred to a 60 mL Teflon line autoclave and then heated at 200 °C for 12 h.

By substituting 5 mL of water from the bespoke approach with H_2O_2 , we propose a novel one-step hydrothermal method for controlling the vacancies. The as-synthesized BFO will be further noted with S3.

Another sample (labeled S2) was prepared by adding a very small amount of bismuth nitrate, 0.1 mmol (0.05 g) more into an identical synthesis procedure as S1.

An XRD PANalytical X’Pert PRO MPD Diffractometer (Almelo, The Netherlands) was used to analyze and identify the samples at room temperature. Using Cu Ka radiation at 40 kV and 30 mA, the XRD characterizations were conducted across the scanning range of 10° to 80°.

Scanning Electron Microscopy (SEM/EDX, Inspect S model, Eindhoven, The Netherlands) was used to examine the morphology and microstructure of the samples.

Fourier transform infrared (FT-IR) spectra were acquired on a JASCO-430 Fourier transform spectrometer (Jasco Inc., Tokyo, Japan) using the KBr pellet technique with resolutions ranging from 2000 to 400 cm^{-1} .

Using a three-electrode cell composed of a 0.28 cm^2 BFO film as the working electrode and a 0.28 cm^2 Ag/AgCl/KCl satellite electrode linked to a Luggin capillary as the reference electrode, electrochemical investigations were carried out using a potentiostat model PGZ 402 (Volatalab, France).

After being combined with a binder solution of polyvinyl alcohol (5% PVA), all three samples were pressed into disks of the same size (6 mm in diameter and approximately 1 mm thick) for the dielectric measurements. These disks were weighted and measured, and densities were determined using Archimedes’ technique, after sintering. The ceramics’ relative densities were calculated as a percentage of the theoretical density [25].

A coating of Ag was placed on both polished surfaces of the disks, representing the two electrodes that were connected to an LCR meter. Complex impedance measurements were performed at various frequencies between 100 Hz and 2 kHz to establish the frequency dependence of the dielectric constant, dielectric loss, and electrical resistance.

3. Results and Discussion

Figure 1 shows the X-ray diffraction pattern of BFO powders prepared using the hydrothermal technique. BiFeO_3 (JCPDS no. 01-072-2321) with a rhombohedral structure is indexed for all diffraction peaks of S1 not highlighting the development of the impurity phases during the synthesis procedure. Both samples S2 and S3 exhibited the development of $\text{Bi}_{25}\text{FeO}_{40}$ impurity phases. The excess oxygen provided by hydrogen peroxide stabilized the $\text{Bi}_{25}\text{FeO}_{40}$ phase in S3. Using the XRD data, the levels of the impurity phases were roughly quantified, with an impurity content of 13% for both. S2, characterized by the same concentration of the impurity phase of $\text{Bi}_{25}\text{FeO}_{40}$ as S3, was used as a standard to exclude the effect of this phase on the structural or electrical characteristics of BFO, highlighting only the effect of hydrogen peroxide on the concentration of vacancies in the BFO structure. According to the first-principles density functional theory calculations [11], the presence of Bi vacancies will change the structural parameters and will be responsible for crystal volume reduction. The quantitative XRD data analysis results using Rietveld refinement (Figure 2) with X'Pert HighScore Plus revealed that the crystal volume of S3 (373.75 \AA^3) is higher than S1 (373.39 \AA^3) and can be correlated with the reduction of Bi vacancies by using hydrogen peroxide in the hydrothermal synthesis.

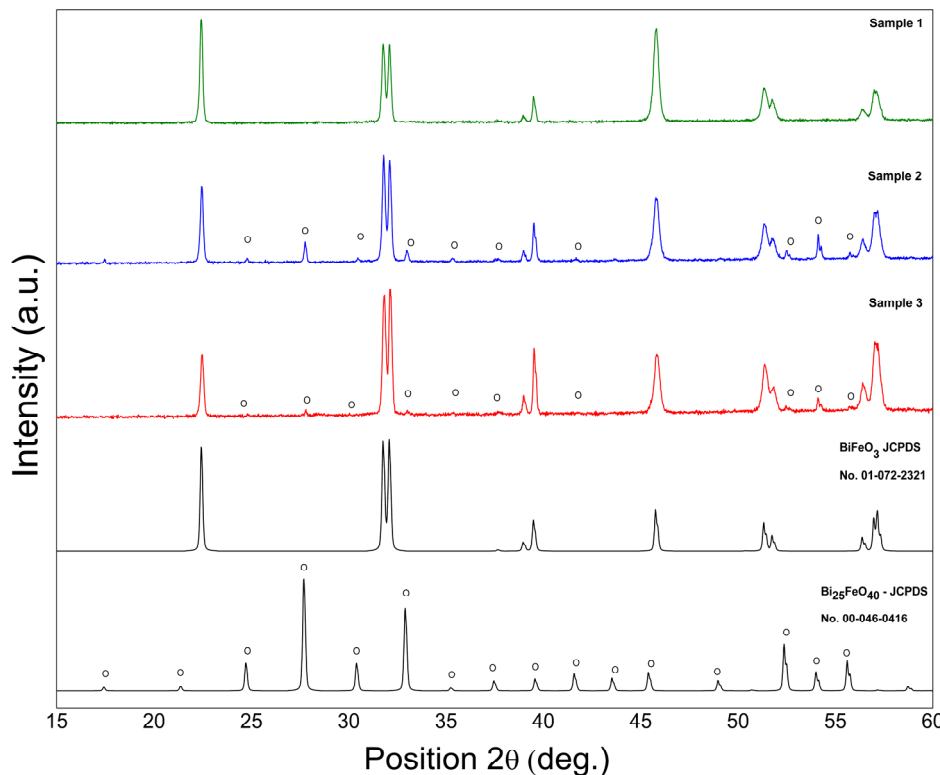


Figure 1. Room temperature X-ray diffraction pattern of BFO powders.

SEM scans (Figure 3a–c) reveal that the resultant BFOs are large-scale aggregations of truncated and highly deformed polyhedra with an average edge length of roughly $10\text{ }\mu\text{m}$. Moreover, no difference in the size or morphology of the produced BFO ceramics by a hydrothermal route with and without hydrogen peroxide was observed.

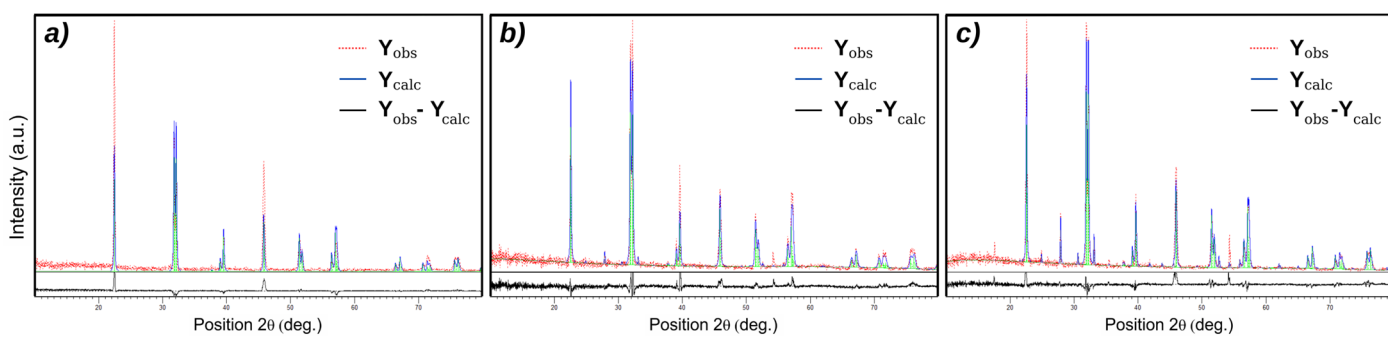


Figure 2. Rietveld refinement of the (a) Sample 1, (b) Sample 2 and (c) Sample 3.

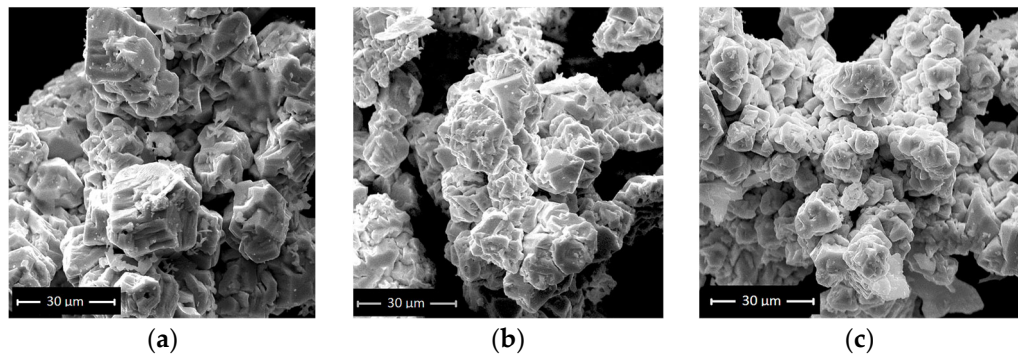


Figure 3. SEM image of (a) sample 1, (b) sample 2 and (c) sample 3.

Table 1 shows the crystalline phases of the final products, as well as the key synthesis parameters that were modified from the standard technique.

Table 1. Crystalline phases of the final products and some synthesis parameters.

Product	Procentage of $\text{BiFeO}_3/\text{Bi}_{25}\text{FeO}_{40}$	Quantity of $\text{H}_2\text{O}_2/\text{H}_2\text{O}$ (mL)	Steering in Closed Conditions	BiFeO_3 Unit Cell Parameters (Å)
S1	100 (%) / 0 (%)	0/15	No	5.576 (7) 5.576 (7) 13.864 (2)
S2	87 (%) / 13 (%)	0/15	No	5.578 (3) 5.578 (3) 13.865 (7)
S3	87 (%) / 13 (%)	5/10	Yes	5.579 (2) 5.579 (2) 13.867 (6)

In contrast to the XRD analysis, a FTIR analysis is much more sensitive to the presence of defects, providing direct information about the modification of the structure of BFO ceramics due to vacancies. The FT-IR spectra of the samples is presented in Figure 4. For all samples, the bands centered at 1640 cm^{-1} correspond to the O-H stretching modes of interlayer water molecules and the bending mode of water molecules $\delta(\text{H}_2\text{O})$, respectively [26,27].

From the viewpoint of V_{Bi} , the region of $650\text{--}400 \text{ cm}^{-1}$, corresponding to the vibration modes of the FeO_6 octahedron, is interesting for analysis. Each sample highlights the two modes of BFO caused by the O-Fe-O bending vibration, $E(TO8)$ and Fe-O stretching vibration, $E(TO9)$. In addition, the absorption peak of S2 and S3 detected at 572 cm^{-1} is the vibrational “fingerprint” of $\text{Bi}_{25}\text{FeO}_{40}$ and corresponds to the stretching vibration of the Fe-O bond [28]. It can be seen that the O-Fe-O bending vibration of BFO is not affected by

hydrogen peroxide or the $\text{Bi}_{25}\text{FeO}_{40}$ phase, being identifiable at approximately 452 cm^{-1} for all three BFOs (Figure 5a).

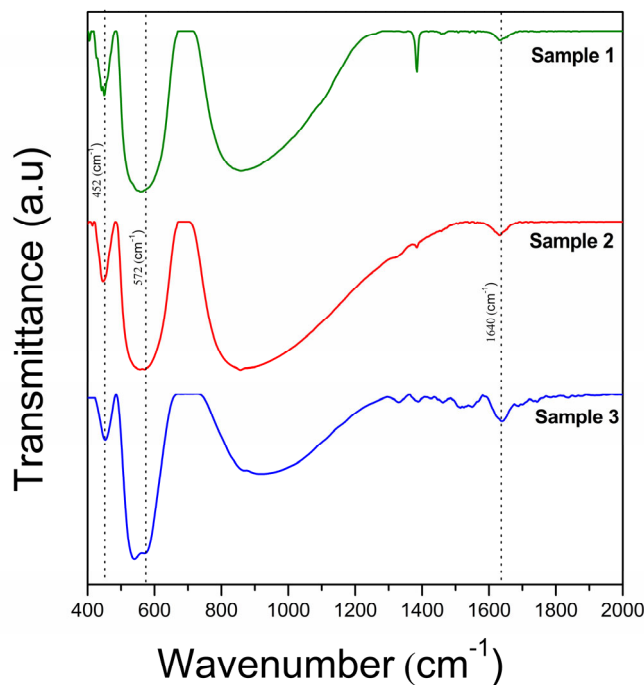


Figure 4. FT-IR spectra of the samples in the range of $400\text{--}2000\text{ cm}^{-1}$.

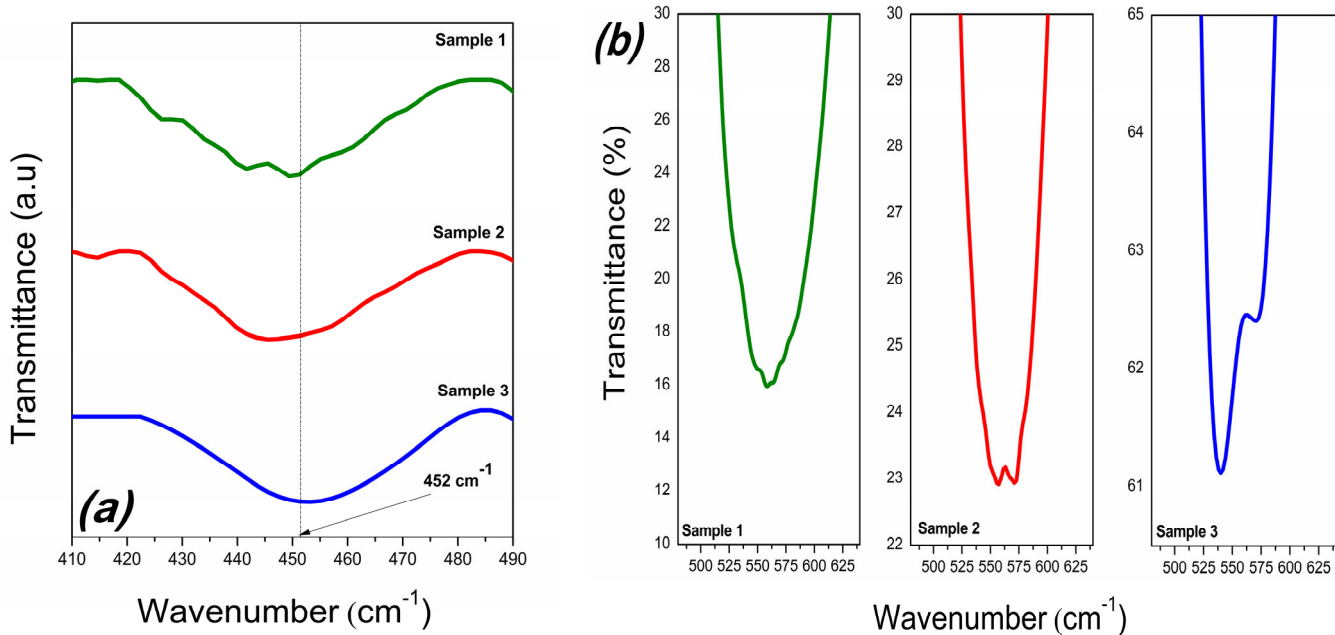


Figure 5. FT-IR spectra of the samples in the range of $400\text{--}490\text{ cm}^{-1}$ (a) and in the range of $480\text{--}640\text{ cm}^{-1}$ (b).

On the contrary, the stretching vibration of the Fe–O bond of BFO changed from 555 cm^{-1} for S1 and S2, respectively, to 538 cm^{-1} for S3 (Figure 5b). From the first-principles calculations, compared to perfect structures, the presence of a Bi vacancy reduces the Fe–O bond [29].

The bond lengths (r) for all the samples were calculated from the values of the force constant (k), using Equations (1) and (2) [28].

$$f = \frac{1}{2\pi} \sqrt{\frac{k}{\mu}} \quad (1)$$

$$k = \frac{17}{r^3} \quad (2)$$

where f is the vibration frequency and μ is the effective mass (2.0644×10^{-26} kg).

The interatomic bond length, Fe-O, is much longer in S3 (2 Å) than in S1 or S2 (≈ 1.96 Å) (Table 2), confirming the reduction of V_{Bi} in the sample synthesized by the hydrogen peroxide-assisted hydrothermal method.

Table 2. Fe-O bond length for all samples.

	Wave Number ν (cm $^{-1}$)	Force Constant k (N/cm)	Bond Length R (Å)
Sample 1	556	2.243	1.957
Sample 2	555	2.259	1.959
Sample 3	538	2.123	2

Moreover, for all three samples, the Mott–Schottky analysis of the BiFeO₃ phase showed a negative slope, indicating *p-type* conductivity. S1, synthesized without H₂O₂, was characterized in our previous work [24]. The *p-type* semiconductor behavior is a characteristic of BFO synthesized by the hydrothermal method in an oxidizing medium, generating Bi vacancies, which, by ionization, release their holes [16]. In addition, the *n-type* conductivity specific to Bi₂₅FeO₄₀ is highlighted by the Mott–Schottky analysis of S3 (Figure 6) [30].

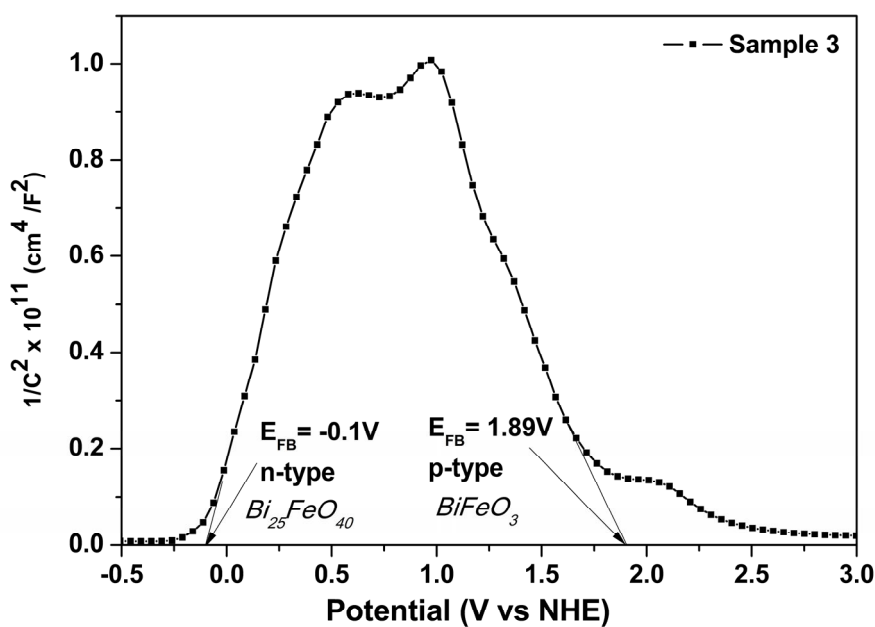


Figure 6. Mott–Schottky plot of Sample 3.

For highlighting the number of h^+ responsible by the *p-type* conduction of the BFO phase, the Mott–Schottky equation [31] has been used to calculate the acceptor density (N_A)

from the slope of the linear region, considering that the dielectric constant of BFO material is 120 in the following equation [32]:

$$N_A = -\frac{2}{e\epsilon\epsilon_0} \left[\frac{d(C^{-2})}{dV} \right]^{-1}$$

where C is defined as the capacitance of the space charge region, ϵ_0 and ϵ are the vacuum permittivity and dielectric constant of BFO, respectively, e is the electron charge and V is the electrode applied potential. The hole density value of S1 is $7.57 \times 10^{17} \text{ cm}^{-3}$ and for S3 this is reduced to $3.49 \times 10^{17} \text{ cm}^{-3}$, confirming the beneficial effect of hydrogen peroxide on defect control in BiFeO_3 semiconductors, even in the case of Bi vacancies.

The characteristics of BFO ceramics are heavily influenced by factors such as grain size and density. The observed results suggest that the experimental conditions used in the synthesis are suitable for the production of highly dense ceramics. Sample 2 has the highest degree of densification (relative density of 93%), while samples 1 and 3 have comparable values ($\approx 92\%$). The high relative densities of all samples rule out any effect of disk preparation on the electrical studies.

Figure 7 depicts the frequency dependence of the dielectric constant (ϵ) and loss ($\tan \delta$) of the samples. It can be seen that both the dielectric constant (ϵ) and loss ($\tan \delta$) of S3 are lower than that of the samples prepared without hydrogen peroxide.

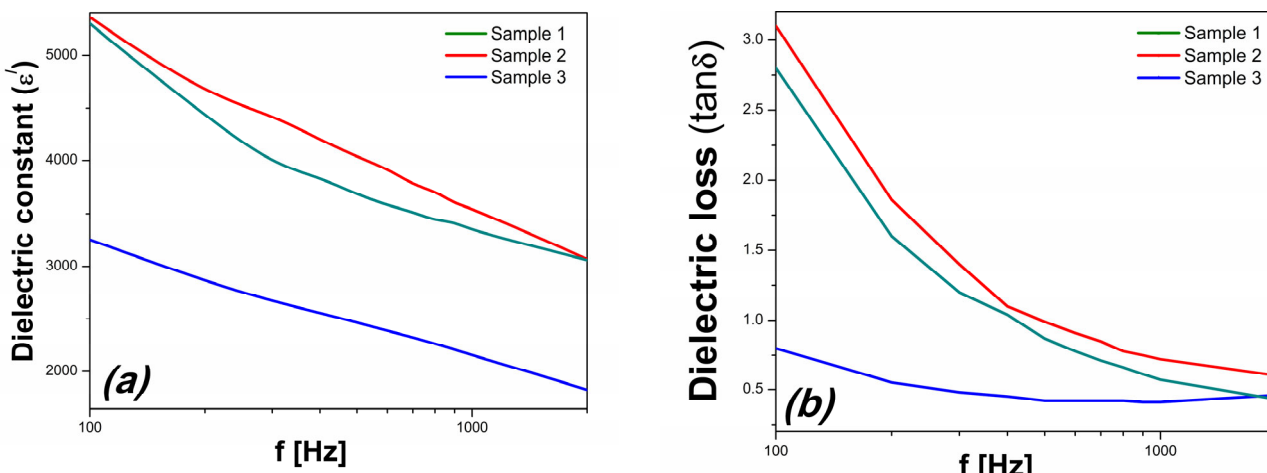


Figure 7. The frequency dependence of (a) the dielectric constant and (b) dielectric loss.

The values of the dielectric constant of S3 are smaller with approximately 40%, while the dielectric loss has an even more substantial decrement being more than 3 times smaller than those of the other two samples. S1 and S2 also have a much stronger dependence on frequency for the dielectric loss than S3, indicating that the leakage current had a significant influence on the dielectric properties of the first two [33]. The very low dielectric loss of S3 is in concordance with the evolution of electrical resistivity, which for S3 is more than three times larger than the reference values of S1 and S2 at 100 Hz.

These very low values of dielectric loss are in agreement with the values presented in Figure 8, where it can be seen that the electrical resistance of Sample 3 is more than three times larger at 100 Hz than the reference values of Samples 1 and 2.

The reduction of Bi vacancies highlighted by the FT-IR and Mott–Schottky analysis has an expected contribution to the dielectric characteristic, decreasing the dielectric constant and loss together with an increase of the electrical resistivity achieved by the H_2O_2 -synthesised BFO ceramic. Furthermore, the similar dielectric behaviors of S1 and S2 reveal that the presence of the $\text{Bi}_{25}\text{FeO}_{40}$ parasitic phase does not significantly affect dielectric properties.

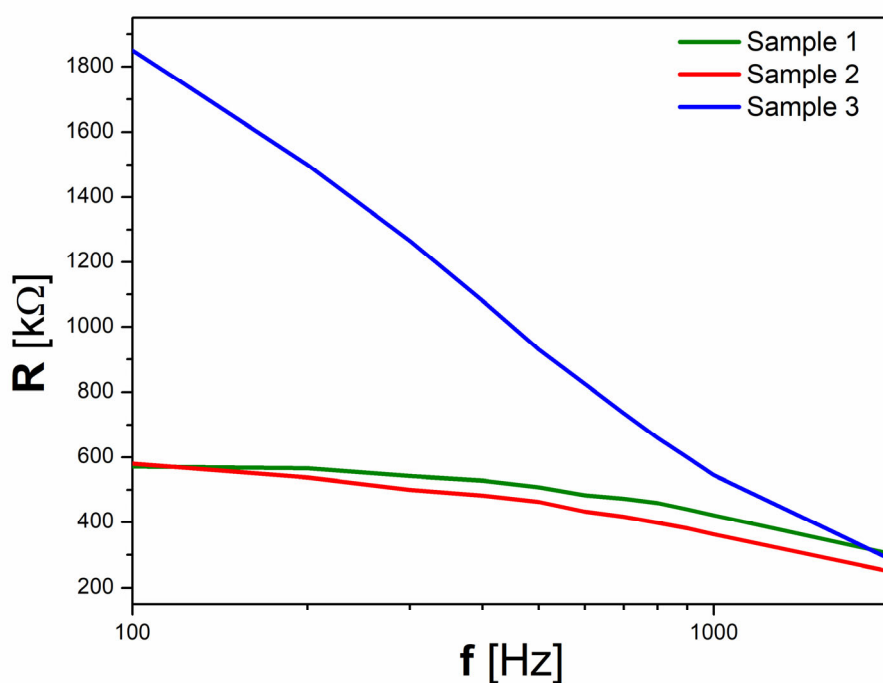
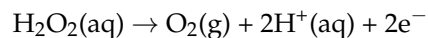


Figure 8. The frequency dependence of electrical resistance.

Taking into consideration the above results, a possible explanation is that hydrogen peroxide (H_2O_2) acted as the electron donor as in the following:



The electrons provided by the donor H_2O_2 compensate the h^+ generated by the unoccupied acceptor V_{Bi} , effectively diminishing the concentration of h^+ and, therefore, leading to an increase in electrical resistivity. In addition, excess oxygen provided by hydrogen peroxide stabilized the $\text{Bi}_{25}\text{FeO}_{40}$ phase in S3.

4. Conclusions

Using hydrogen peroxide (H_2O_2) as part of a hydrothermal medium, *p*-type BiFeO_3 ceramics characterized by high electrical resistivity have been obtained. FT-IR and Mott-Schottky analyses highlighted the reduction of V_{Bi} in the sample synthesized by the hydrogen peroxide-assisted hydrothermal method. Thus, the interatomic bond length, Fe-O, is much longer in S3 (2 Å) than in S1 or S2 (1.96 Å). This, together with the reduction of the hole density value to $7.57 \times 10^{17} \text{ cm}^{-3}$ in the case of S1 and to $3.49 \times 10^{17} \text{ cm}^{-3}$ in the case of S3, confirms the beneficial effect of hydrogen peroxide on the defect control in BiFeO_3 semiconductors, even in the case of Bi vacancies. The reduction of Bi vacancies has an expected contribution to the dielectric characteristic, namely decreasing the dielectric constant and loss, together with an increase of electrical resistivity. Furthermore, the similar dielectric behaviors of S1 and S2 reveal that the presence of the $\text{Bi}_{25}\text{FeO}_{40}$ parasitic phase does not significantly affect the dielectric properties. In conclusion, hydrogen peroxide (H_2O_2) acted as the electron donor. The electrons provided by the donor H_2O_2 compensated the h^+ generated by the unoccupied acceptor V_{Bi} , leading to a decrease in the concentration of h^+ . Enhancing the dielectric and electrical properties achieved by the H_2O_2 -synthesised BFO ceramic confirms that bismuth vacancies can be reduced by this method. In our future work, we will study the effect of the amount of hydrogen peroxide on Bi vacancies, reflecting on the dielectric and electrical properties. In addition, the hydrogen peroxide-assisted hydrothermal synthesis might be extended to the synthesis of other perovskite materials.

Author Contributions: Conceptualization, C.C. and I.M.; Methodology, C.C., R.B. and D.U.; Validation, C.C., D.U. and I.M.; Investigation, R.B., D.U. and I.M.; Writing—review & editing, M.M.; Supervision, M.M. All authors have read and agreed to the published version of the manuscript.

Funding: This work was funded by a grant from the Ministry of Research, Innovation and Digitization, CCCDI-UEFISCDI (project number PN-III-P2-2.1-PED-2021-0624) within PNCDI III.

Institutional Review Board Statement: Not applicable.

Informed Consent Statement: Not applicable.

Data Availability Statement: The data presented in this study are available upon request from the corresponding author.

Conflicts of Interest: The authors declare no conflict of interest.

References

- Martin, L.W.; Crane, S.P.; Chu, Y.-H.; Holcomb, M.B.; Gajek, M.; Huijben, M.; Yang, C.-H.; Balke, N.; Ramesh, R. Multiferroics and magnetoelectrics: Thin films and nanostructures. *J. Phys. Condens. Matter* **2008**, *20*, 434220–434233. [[CrossRef](#)]
- Deka, B.; Cho, K.H. BiFeO₃-Based Relaxor Ferroelectrics for Energy Storage: Progress and Prospects. *Materials* **2021**, *14*, 7188. [[CrossRef](#)]
- Catalan, G.; Scott, J.F. Physics and applications of bismuth ferrite. *Adv. Mater.* **2009**, *21*, 2463–2485. [[CrossRef](#)]
- Rojac, T.; Bencan, A.; Malic, B.; Tutuncu, G.; Jones, J.L.; Daniels, J.E.; Damjanovic, D. BiFeO₃ ceramics: Processing, electrical, and electromechanical properties. *J. Am. Ceram. Soc.* **2014**, *97*, 1993–2011. [[CrossRef](#)]
- Zhou, X.; Sun, H.; Luo, Z.; Zhao, H.; Liang, D.; Jafri, H.M.; Huang, H.; Yin, Y.; Li, X. Ferroelectric diode characteristic and tri-state memory in self-assembled BiFeO₃ nanoislands with cross-shaped domain structure. *Appl. Phys. Lett.* **2022**, *121*, 042903. [[CrossRef](#)]
- Chen, G.; Chen, J.; Pei, W.; Lu, Y.; Zhang, Q.; Zhang, Q.; He, Y. Bismuth Ferrite Materials for Solar Cells: Current Status and Prospects. *Mater. Res. Bull.* **2019**, *110*, 39–49. [[CrossRef](#)]
- Kadim, G.; Masrour, R.; Jabar, A. Ferroelectric, quantum efficiency and photovoltaic properties in perovskite BiFeO₃ thin films: First principle calculations and Monte Carlo study. *Int. J. Energy Res.* **2021**, *45*, 9961–9969. [[CrossRef](#)]
- Radmilovic, A.; Smart, T.J.; Ping, Y.; Choi, K. Combined Experimental and Theoretical Investigations of n-Type BiFeO₃ for Use as a Photoanode in a Photoelectrochemical Cell. *Chem. Mater.* **2020**, *32*, 3262–3270. [[CrossRef](#)]
- Yang, H.; Wang, Y.Q.; Wang, H.; Jia, X. Oxygen concentration and its effect on the leakage current in BiFeO₃ thin films. *Appl. Phys. Lett.* **2010**, *96*, 012909. [[CrossRef](#)]
- Yang, T.; Wei, J.; Sun, Z.; Li, Y.; Liu, Z.; Xu, Y.; Chen, G.; Wang, T.; Sun, H.; Cheng, Z. Design of oxygen vacancy in BiFeO₃-based films for higher photovoltaic performance. *Appl. Surf. Sci.* **2022**, *575*, 151713. [[CrossRef](#)]
- Xia, L.; Tybell, T.; Selbach, S.M. Bi vacancy formation in BiFeO₃ epitaxial thin films under compressive (001)-strain from first principles. *J. Mater. Chem. C* **2019**, *7*, 4870–4878. [[CrossRef](#)]
- Duan, F.; Ma, Y.; Lv, P.; Sheng, J.; Lu, S.; Zhu, H.; Du, M.; Chen, X.; Chen, M. Oxygen vacancy-enriched Bi₂O₃/BiFeO₃ p-n heterojunction nanofibers with highly efficient photocatalytic activity under visible light irradiation. *Appl. Surf. Sci.* **2021**, *562*, 150171. [[CrossRef](#)]
- Dias, G.S.; Catellani, I.B.; Cotica, L.F.; Santos, I.A.; Freitas, V.F.; Yokaichiya, F. Highly resistive fast-sintered BiFeO₃ ceramics, Integrated Ferroelectrics. *Integr. Ferroelectr.* **2016**, *174*, 43–49. [[CrossRef](#)]
- Wang, N.; Luo, X.; Han, L.; Zhang, Z.; Zhang, R.; Olin, H.; Yang, Y. Structure, Performance, and Application of BiFeO₃ Nanomaterials. *Nano-Micro Lett.* **2020**, *81*, 12. [[CrossRef](#)] [[PubMed](#)]
- Wang, Y.F.; Xu, C.; Yan, L.; Qiao, X. Precise Adjustment of Forbidden Bandwidth in BiFeO₃ / Bi₂₅FeO₄₀ Heterojunction Structure. *SSRN* **2022**. [[CrossRef](#)]
- Xu, Q.; Sobhan, M.; Yang, Q.; Anariba, F.; Ong, K.P.; Wu, P. The role of Bi vacancies in the electrical conduction of BiFeO₃: A first-principles approach. *Dalton Trans.* **2014**, *43*, 10787–10793. [[CrossRef](#)] [[PubMed](#)]
- Tuluk, A.; Brouwer, H.; van der Zwaag, S. Controlling the Oxygen Defects Concentration in a Pure BiFeO₃ Bulk Ceramic. *Materials* **2022**, *15*, 6509. [[CrossRef](#)]
- Yang, T.; Wei, J.; Lv, Z. Ferroelectric polarization tuning the photovoltaic and diode-like effect of the Ni, Sm co-doped BiFeO₃ film capacitors. *J. Mater. Sci. Mater. Electron.* **2019**, *30*, 12163–12169. [[CrossRef](#)]
- Imaizumi, F.; Goto, T.; Teramoto, A.; Sugawa, S.; Ohmi, T. Crystallinity improvement of ferroelectric BiFeO₃ thin film by oxygen radical treatment. *ECS Trans.* **2015**, *66*, 261–267. [[CrossRef](#)]
- Martínez, A.B.; Godard, N.; Aruchamy, N.; Milesi-Brault, C.; Condurache, O.; Bencan, A.; Glinsek, S.; Granzow, T. Solution-processed BiFeO₃ thin films with low leakage current. *J. Eur. Ceram. Soc.* **2021**, *41*, 6449–6455. [[CrossRef](#)]
- Syed, A.; Siddaramanna, A.; Elgorban, A.M.; Hakeem, D.A.; Nagaraju, G. Hydrogen Peroxide-Assisted Hydrothermal Synthesis of BiFeO₃ Microspheres and Their Dielectric Behavior. *Magnetochemistry* **2020**, *6*, 42. [[CrossRef](#)]
- Geneste, G.; Paillard, C.; Dkhil, B. Polarons, vacancies, vacancy associations, and defect states in multiferroic BiFeO₃. *Physical. Review B* **2019**, *99*, 024104. [[CrossRef](#)]

23. Peng, Y.-T. Remarkably enhanced photovoltaic effects and first-principles calculations in neodymium doped BiFeO₃. *Sci. Rep.* **2017**, *7*, 45164. [[CrossRef](#)] [[PubMed](#)]
24. Casut, C.; Bucur, R.; Miclau, N.; Malaescu, I.; Miclau, M. Biphasic BiFeO₃ ceramics based on rhombohedral and tetragonal polymorphs. *Adv. Appl. Ceram.* **2023**. [[CrossRef](#)]
25. Bucur, R.; Bucur, A.I.; Novacconi, S.; Nicoara, I. Synthesis and characterization of BaTi_{1-x}Sn_xO₃-0.5mol%GeO₂. *J. Alloy Compd.* **2012**, *539*, 148–153. [[CrossRef](#)]
26. Čebela, M.; Jankovic, B.; Hercigonja, R.; Lukic, M.J.; Dohcevic-Mitrovic, Z.; Milivojevic, D.; Matovic, B. Comprehensive characterization of BiFeO₃ powder synthesized by the hydrothermal procedure. *Process. Appl. Ceram.* **2016**, *10*, 201–208. [[CrossRef](#)]
27. Mukherjee, A.; Hossain, S.M.; Pal, M.; Basu, S. Effect of Y-doping on optical properties of multiferroics BiFeO₃ nanoparticles. *Appl. Nanosci.* **2012**, *2*, 305–310. [[CrossRef](#)]
28. Zhang, L.; Zou, Y.; Song, J.; Pan, C.-L.; Sheng, S.-D.; Hou, C.-M. Enhanced photocatalytic activity of Bi₂₅FeO₄₀-Bi₂WO₆ heterostructures based on the rational design of the heterojunction interface. *RSC Adv.* **2016**, *6*, 26038–26044. [[CrossRef](#)]
29. Shah, N.M.; Patel, N.H.; Shah, D.D.; Mehta, P.K. FTIR: Important tool to investigate the chemical bond formation in the polycrystalline xBaTiO₃—(1-x)BiFeO₃. *Mater. Today: Proc.* **2021**, *47*, 616–620. [[CrossRef](#)]
30. Zhang, R.; Zhang, T.; Zhao, C.; Han, Q.; Li, Y.; Liu, Y.; Zeng, K. A novel Z-scheme Bi₂WO₆-based photocatalyst with enhanced dye degradation activity. *J. Nanoparticle Res.* **2019**, *21*, 203. [[CrossRef](#)]
31. Gelderman, K.; Lee, L.; Donne, S.W. Flat-Band Potential of a Semiconductor: W Using the Mott–Schottky Equation. *J. Chem. Educ.* **2007**, *84*, 685–688. [[CrossRef](#)]
32. Zhang, C.; Li, Y.; Chu, M. Hydrogen-treated BiFeO₃ nanoparticles with enhanced photoelectrochemical performance. *RSC Adv.* **2016**, *6*, 24760–24767. [[CrossRef](#)]
33. Gu, Y.H.; Wang, Y.; Chen, F.; Chan, H.L.W.; Chen, W.P. Nonstoichiometric BiFe_{0.9}Ti_{0.05}O₃ multiferroic ceramics with ultrahigh electrical resistivity. *J. Appl. Phys.* **2010**, *108*, 094112. [[CrossRef](#)]

Disclaimer/Publisher's Note: The statements, opinions and data contained in all publications are solely those of the individual author(s) and contributor(s) and not of MDPI and/or the editor(s). MDPI and/or the editor(s) disclaim responsibility for any injury to people or property resulting from any ideas, methods, instructions or products referred to in the content.